SUPPORTING INFORMATION

Supporting Information

69451 Weinheim, Germany

Abstract: The benefits of intracellular drug delivery from nanomedicine has been limited by biological barriers and to some extent targeting capability. We investigated a size-controlled, dual tumor-mitochondria-targeted theranostic nanoplatform (Porphyrin-PEG Nanocomplexes, PPNs). The maximum tumor accumulation (15.6 %ID/g, 72 h p.i.) and ideal tumor-to-muscle ratio (16.6, 72 h p.i.) was achieved using an optimized PPN particle size of approximately 10 nm *via* PET imaging tracing. The stable coordination of PPNs with ^{177}Lu enables integration of fluorescence imaging (FL) and photodynamic therapy (PDT) with positron emission tomography (PET) imaging and internal radiotherapy (RT). Furthermore, efficient tumor and mitochondrial uptake of ^{177}Lu-PPNs greatly enhanced the efficacies of RT and/or PDT. This work developed a facile approach to fabricate tumor-targeted multi-modal nanotheranostic agents, which enables precision and radionuclide-based combination tumor therapy.

DOI: 10.1002/anie.2016XXXXX

SUPPORTING INFORMATION

Table of Contents

Radionuclide-based combination therapy: A dual tumor-mitochondria-targeted theranostic nanoplatform with controllable biodistribution in vivo was fabricated by complexing meso-tetra(4-carboxyphenyl)-porphyrin with 8-arm-amine-polyethylene glycol (PPNs). Efficient cancer theranostics benefit maximally from the co-location of imaging signal and radionuclide-based combination therapy component.

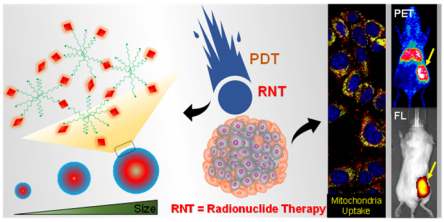

Bo Yu, Hao Wei, Qianjun He, Carolina A. Ferreira, Christopher J. Kutyreff, Dalong Ni, Zachary T. Rosenkrans, Liang Cheng, Faquan Yu, Jonathan W. Engle, Xiaoli Lan*, and Weibo Cai**

Experimental Procedures

Characterization. Transmission electron microscopy (TEM) images were carried on an FEI T12 microscope operated at an accelerating voltage of 120 kV. Standard TEM samples were prepared by dropping diluted products onto carbon-coated copper grids. Dynamic light scattering and Zeta potential were performed on Nano-Zeta sizer (Malvern Instruments Ltd.). Biodistribution analysis were performed by measuring the radioactivity in the tissue in a WIZARD^2 gamma counter (Perkin-Elmer). Optical imaging was performed by using an IVIS Spectrum Preclinical in vivo imaging system (Ex = 640 nm, Em= 740 nm).

Synthesis of PPNs. PPNs with various sizes were synthesized using a simple amide coupling reaction. Briefly, meso-tetra(4-carboxyphenyl)-porphyrin (mTCPP, Sigma-Aldrich), 8-arm-amine-polyethylene glycol (aPEG) (molecular weight 20 K, Creative PEGworks), and 1-ethyl-3-(3-dimethylaminopropyl) carbodiimide hydrochloride (EDC, ThermoFishser) (the molar ratio of mTCPP: 8Arms-PEG: EDC was 1:2:4) was added to the 50 mL of DMSO at room temperature under argon gas protection. After reaction for a fixed time, the products were collected and dialyzed in water for 14 days. The products were further collected by ultrafiltration (cutoff 100 K). The samples were then collected by frozen-dry.

^{64}Cu-labeling. ^{64}Cu was produced with an onsite cyclotron (GE PETrace) at the University of Wisconsin-Madison. $^{64}CuCl_2$ (150 MBq) was diluted in 0.1 M sodium acetate buffer (pH 5.5) and mixed with 100 μL of PPNs. The reaction was conducted at 70 °C for 120 min with constant shaking. TLC determined the labeling yield at different time points using 50 mM EDTA solution as the mobile phase. Fluorescence imaging was performed by utilizing an IVIS Spectrum. The resulting product was purified using a PD-10 column with PBS as the mobile phase.

^{177}Lu-labeling. ^{177}Lu was obtained from Perkin Elmer. $^{177}LuCl_3$ (150 MBq) was diluted in 0.1 M sodium acetate buffer (pH 5.5) and mixed with 100 μL of PPNs. The reaction was conducted at 70 °C for 120 min with constant shaking. TLC determined the labeling yield at different time points using 50 mM EDTA solution as the mobile phase. Fluorescence imaging was performed by utilizing an IVIS Spectrum. The resulting product was purified using a PD-10 column with PBS as the mobile phase.

***In Vitro* Serum Stability Study.** For *in vitro* serum stability, ^{177}Lu-PPNs and mouse serum were incubated under constant shaking at 37 ºC for 24 h. Small portions of the mixture were collected at different time points and purified using 100 kDa cutoff filters. After filtering, the solutions were collected, and the radioactivity of ^{177}Lu was measured by using a gamma counter.

MTT assay. 4T1 cells (1×10^4) were seeded in 96-well plates. After 24 h, PPNs-10nm with various concentrations calculated by mTCPP of PPNs based on the fluorescence intensity and then ^{177}Lu-PPNs-10nm were added. For the co-treatment of ^{177}Lu-PPNs-10nm and laser, the radioactivity intensity of ^{177}Lu-PPNs-10nm was 20 μCi. For the ^{177}Lu-PPNs-10nm alone group, the mTCPP concentration of ^{177}Lu-PPNs-10nm was 1 μM. After incubation for 6 h, the cells were washed with PBS, and the fresh cell culture medium was added. The experimental groups were then exposed to 660 nm laser irradiation under a power density of 20 mW/cm^2 for 10 min. Finally, all samples were incubated in the dark for another 12 h.

Cellular internalization of PPNs. Briefly, the cells cultured on cover glass in 6-well plates till 70% confluence were stained with Hoechst 33324 for 20 min. Then washing with PBS, the cells were treated with different concentrations of PPNs-10nm for various periods of time, Then the cells were fixed in 4% paraformaldehyde and visualized with a Nikon A1RS confocal microscope.

Intracellular localization of PPNs. After stained with Hoechst 33324, the cells were incubated with PPNs-10nm for various periods of time. The MitoTracker Green FM was added and continued to incubate for another 30 min. Cells were washed with DMEM medium for 3 times before imaging with a Nikon A1RS confocal microscope.

SUPPORTING INFORMATION

In vitro oxidative stress detection. After incubation with various materials for 6 h, the cells were washed with PBS and the fresh culture medium of cell was added then the cells were treated with or without the laser. CellROX™ green reagent (Invitrogen) was used to analyze the oxidative stress in cells after treatment with PPNs-10nm (20 μM), ^{177}Lu-PPNs-10nm (20 μCi, 20 μM), PPNs-10nm (20 μM) + 660 nm laser (20 mW/cm^2 for 10 min), and ^{177}Lu-PPNs-10nm (20 μCi, 20 μM) 660 nm laser (20 mW/cm^2 for 10 min).

In vitro mitochondrial mass assay. After stained with Hoechst 33324, the cells were treated as the oxidative stress detection section. Then the MitoTracker Green FM was added and continued to incubate for another 30 min. Cells were washed with DMEM medium for 3 times before imaging with a Nikon A1RS confocal microscope.

Animal Model. All animal studies were conducted under the protocol approved by the University of Wisconsin Institutional Animal Care and Use Committee.

Immunofluorescent staining of tumor tissues. Tumors were collected 2 days and 6 daysp.i. of PPNs-10nm. Tissues were embedded and frozen in Optimal Cutting Temperature compound (Sakura Fintek) and sectioned into 7 μm slices. Immunofluorescent staining was performed on tumor tissues to look for the presence of angiogenesis and the existing blood vessel structure, using AlexaFluor488-conjugated anti-CD31.

***In Vivo* PET Imaging and Biodistribution Studies.** For normal PET imaging, 4T1 tumor-bearing BALB/c mice were injected with ^{64}Cu-PPNs via the tail vein before serial PET scans. Quantitative PET data was presented as a percentage of the injected dose per gram (%ID/g). For biodistribution studies, major organs were collected and wet-weighed at designed time points p.i. The radioactivity uptake by the tissue was measured by using a gamma-counter (Perkin-Elmer) and presented as %ID/g (mean ± SD).

Ex vivo Imaging of Main Organs. The mice were sacrificed at designed times, the main organs (heart, liver, spleen, pancreas, lung, kidney, stomach, and intestine) were harvested at different time point for ex vivo PET imaging or fluorescence imaging (using a 640 nm/740 nm excitation/emission filter).

***In vivo* Therapy.** For in vivo photodynamic therapy, 4T1 tumor-bearing mice were randomly divided into five treatment groups: the first group was injected with PBS (150 μL); the second group was intravenously injected with free ^{177}Lu in PBS (200 μL, 200 μCi); the third group was intravenously injected with PPNs-10nm (200 μL, 1 mg/mL) with 660 nm laser irradiation; the fourth group was intravenously injected with ^{177}Lu-PPNs-10nm (200 μL, 1 mg/mL, labeling with 200 μCi of ^{177}Lu) without 660 nm laser irradiation; the fifth group was intravenously injected with ^{177}Lu-PPNs-10nm (200 μL, 1 mg/mL, labeling with 200 μCi of ^{177}Lu) with 660 nm laser irradiation. PDT treatments were conducted 48 h p.i. with the 660 nm laser at the power density of 40 mW/cm^2 for 20 min. The tumor sizes were measured with a caliper every other day and calculated as volume = (tumor length) × (tumor width)^2/2. Relative tumor volumes were calculated as V/V_0 (V_0 is the initial tumor volume). Body weights were monitored.

Results and Discussion

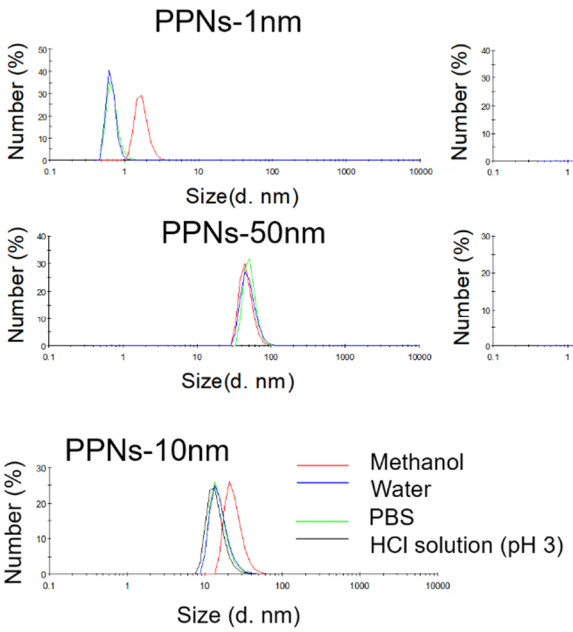

Figure S1. DLS characterization of obtained PPNs and obtained PPNs-10nm dispersed in different solvents. We estimated the DLS size of obtained PPNs-10nm dispersed in different solvents. The diameter of PPNs-10nm were found to remain approximately the same in each of the tested solvents.The diameter increased after being dispersed in pure methanol, which may be due to the ability of methanol to enter the internal part of nanoparticles. The final products aggregated into a bulk gel when the reaction time achieved 120 h (**Figure 1b**). On the contrary, PPNs-10nm were extremely stable even after 2 months. It was previously found that the PPN mesh exists in a loosely defined self-assembly of very small polymers, as the molecular weight of used PEG was small [1]. However, in this experiment, the hydrophilic ability of using bigger PEG (20 kDa) might inhibit the weak self-assembly. Thus, we believe that the PPNs was formed by chemical conjugation.

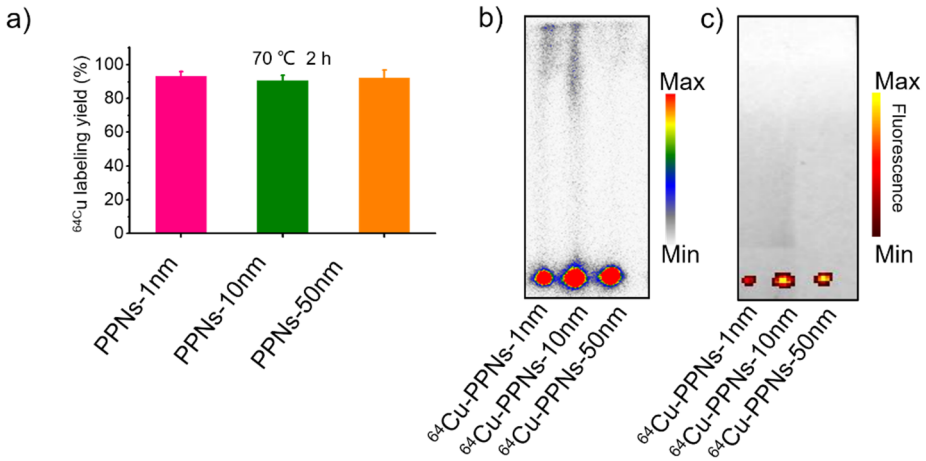

Figure S2. a) Labeling yield of obtained PPNs after incubating with ^{64}Cu in the acid buffer for 2 h at 70 ℃ (n=3). b) TLC radioactivity imaging. c) Fluorescence imaging (mTCPP acted as the fluorescence molecule).

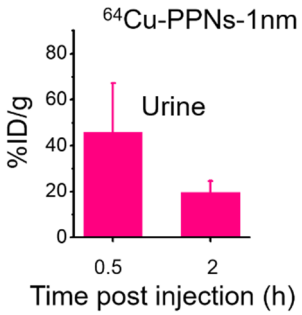

Figure S3. Quantitative data obtained from ROI analysis of PET images. The radioactivity signal in the urine or bladder was decreased from 45.9±21.1 %ID/g (0.5 h) to be 19.6±5.0 %ID/g (2 h) (n=3). The imaging indicated that obtained ^{64}Cu-PPNs-1nm with small sizes could pass through the kidneys for rapid clearance.

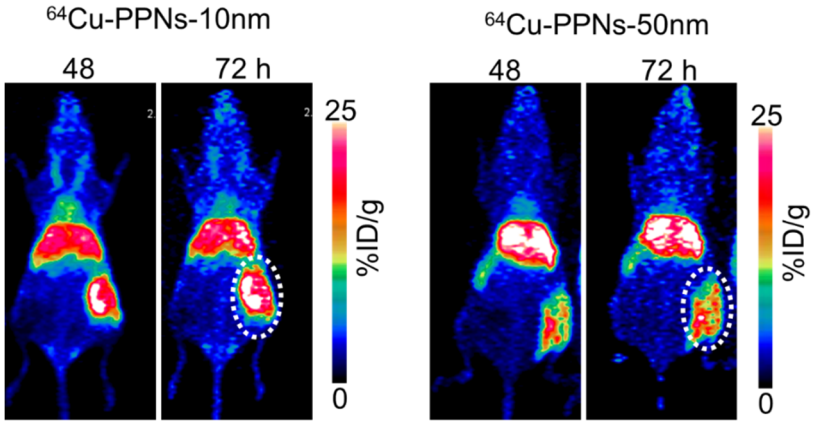

Figure S4. Maximum intensity projections (MIP) of PET images of ^{64}Cu-PPNs-10nm and ^{64}Cu-PPNs-50nm. The final tumor uptake of ^{64}Cu-PPNs (10 nm, 50 nm) reached 15.6 ± 1.3 %ID/g and 7.5 ± 1.0 %ID/g, respectively. The elevated tumor uptake of ^{64}Cu-PPNs-10nm was attributed to the enhanced blood circulation.

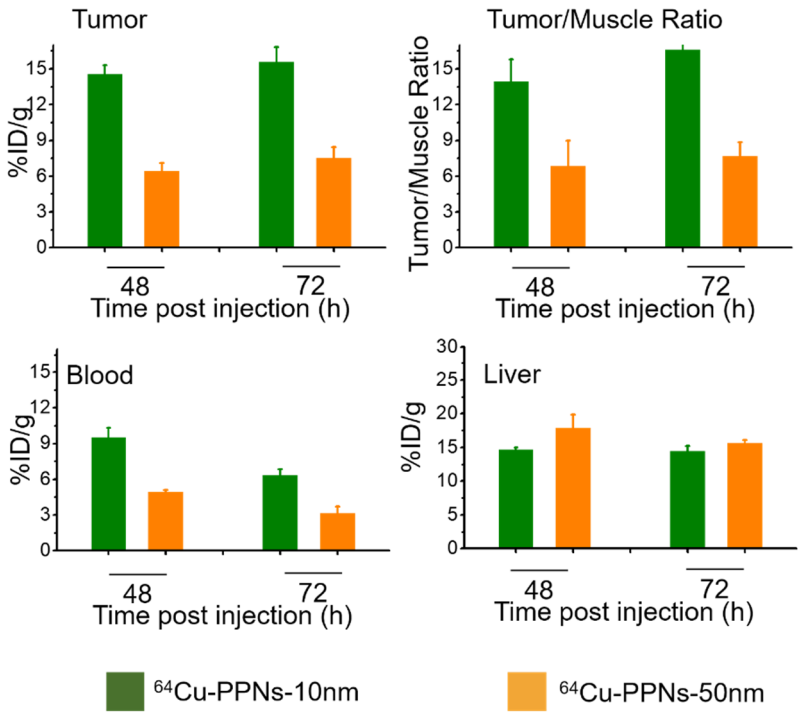

Figure S5. Quantitative data obtained from ROI analysis of PET images of ^{64}Cu-PPNs-10nm and ^{64}Cu-PPNs-50nm respectively (n=3).

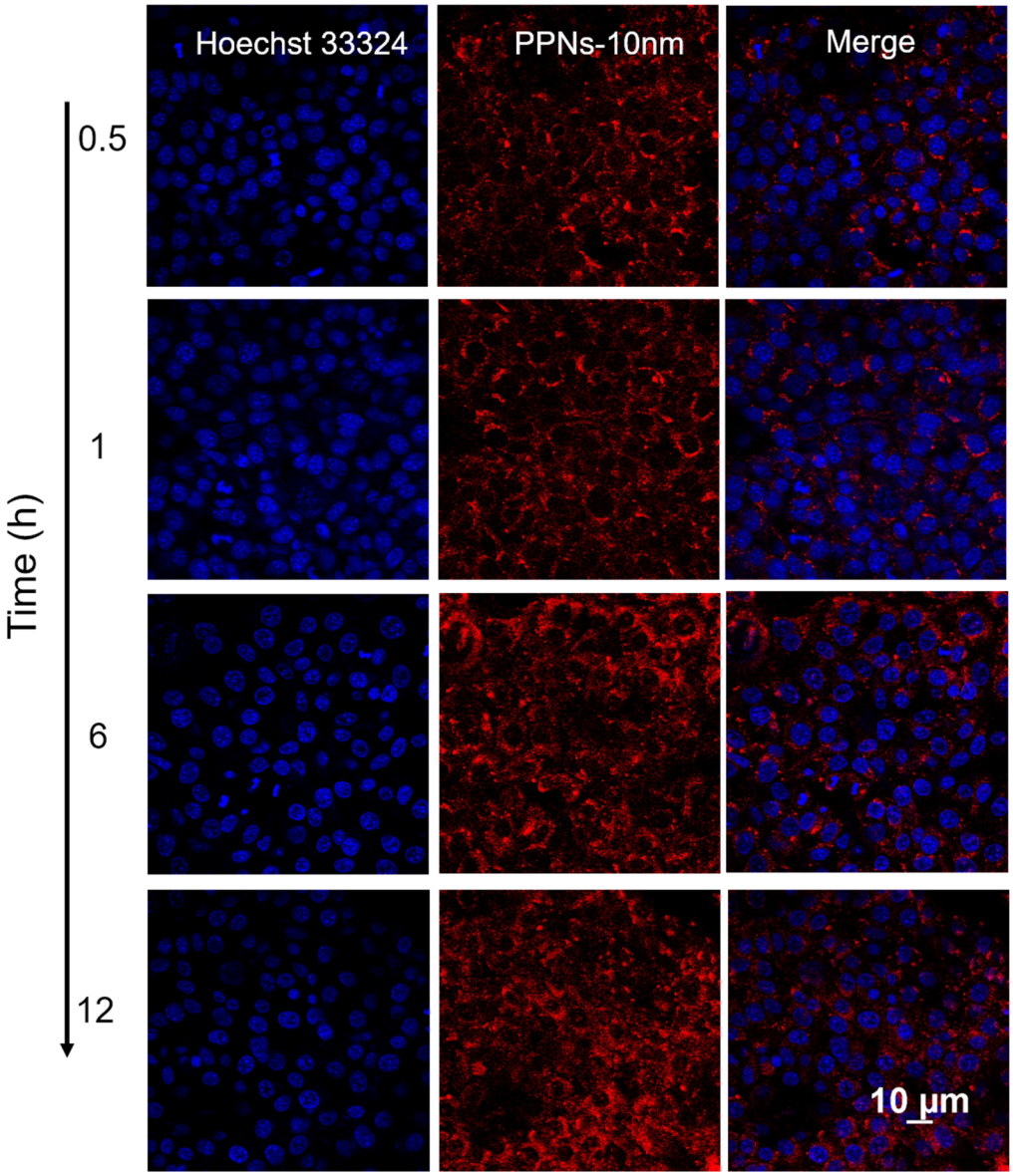

Figure S6. Confocal microscopy images of 4T1 cells treated with PPNs-10nm for a different period.

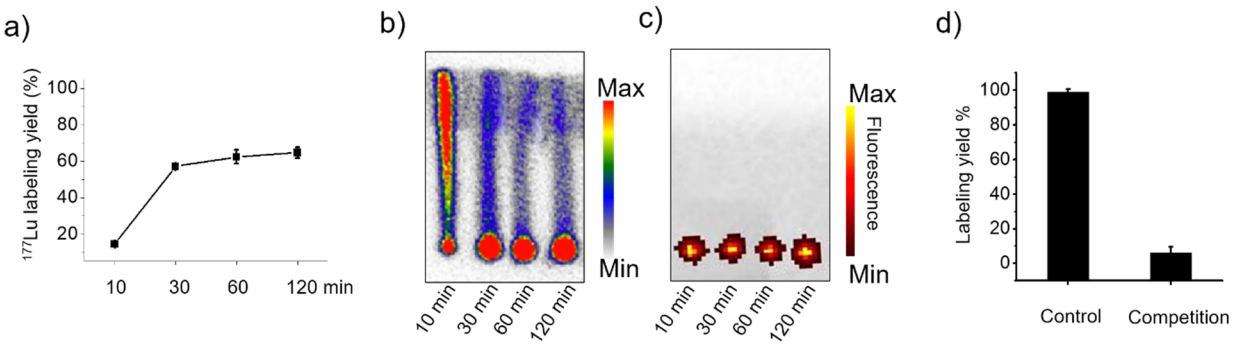

Figure S7. (a) Time-dependent ^{177}Lu-labeling yields of PPNs-10nm. (b) Autoradiograph of TLC plates of ^{177}Lu-PPNs-10nm (n=3). (c) Overlay of the bright field imaging and fluorescence of ^{177}Lu-PPNs-10nm (mTCPP acted as the fluorescence molecule). (d) $LuCl_3$ was diluted in 0.1 M sodium acetate buffer (pH 5.5) and mixed with 100 μL of PPNs (The concentration of mTCP was 0.19 mM). The reaction was conducted at 70 °C for 120 min with constant shaking. The resulting product was purified using a PD-10 column with PBS as the mobile phase. Then the Lu-PPNs was digested by acid.[2] And the Lu concentration was analyzed by ICP-AES. The Lu-labeling yields of PPNs-10nm was set as 100% (**Control group**). Using the same process as described in the preparation of Lu-PPNs except for $CuCl_2$ instead of $LuCl_3$, Cu-PPNs-10nm was synthesized. Using the same process as described in the preparation of Lu-PPNs except for Cu-PPNs-10nm instead of PPNs, the concentration of Lu in **competition group** was analyzed by ICP-AES. And the Lu-labeling yield was calculated by comparing with Lu-PPNs group. It was found the labeling yield of Lu^{3+} was decreased after the macrocycle core of mTCPP was occupied by the Cu^{2+}. Thus, for labeling ^{177}Lu, we noticed that the labeling ability of PNNs is dependent on the components of the whole nano-structure, which is composed of free amino (primary amine) of 8Arm-amino-PEG, cations ring (tertiary amine) of porphyrin, and the free carboxyl group of mTCPP. Aside from the steric-hindrance effect and hybrid state, the primary amine is usually considered a better ligand to form a metal complex than the tertiary amine of a porphyrin. In addition, the chelation of ^{177}Lu by DTPA (diethylene triamine pentaacetic acid) with a linear structure or open-loop hints at multiple possible sites for labeling isotope. It may also be possible that the chelation of ^{177}Lu was dependent on the entire nanocomplexes structure which is comprised of free amino of 8Arm-amino-PEG, cations ring of porphyrin, and free carboxyl group of mTCPP.

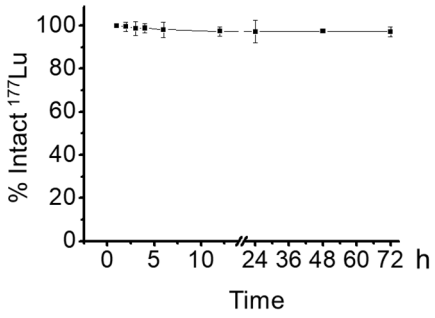

Figure S8. Serum stability study of ^{177}Lu-PPNs-10nm in the whole mouse serum at 37 ℃ (n=3).

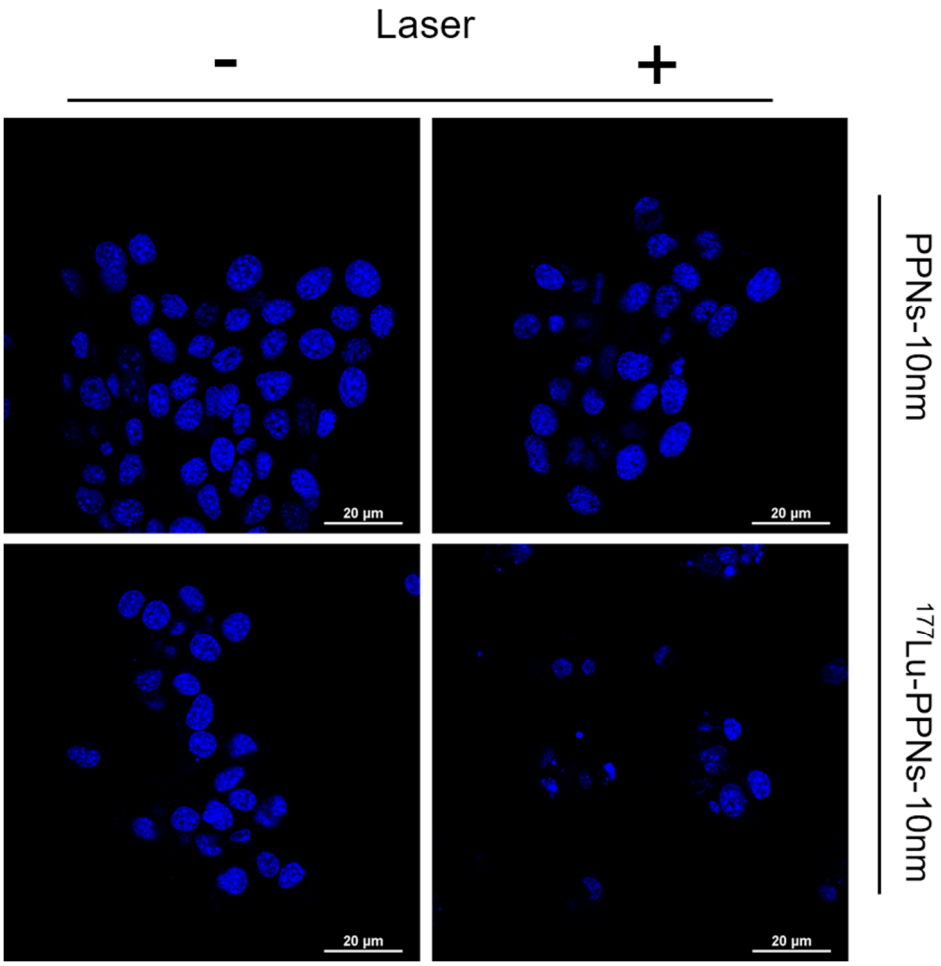

Figure S9. Cell nucleus condensation after treatment. The nucleus was stained with Hoechst 33324.

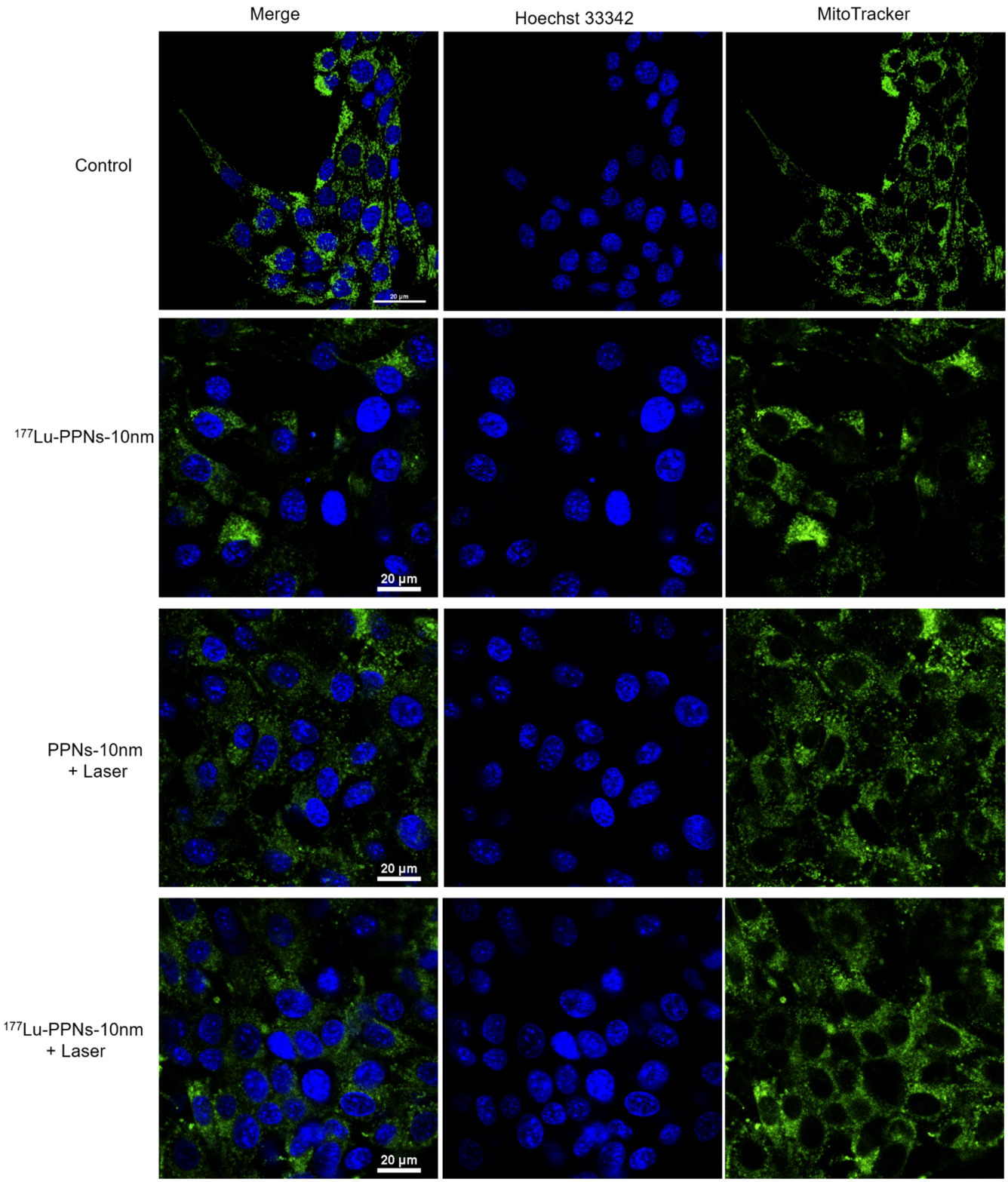

Figure S10. The morphological change of mitochondria in cells after treatments. The cells were stained with Hoechst 33342 (blue) and MitoTrackerGreen (green) and observed using laser scanning confocal microscopy.

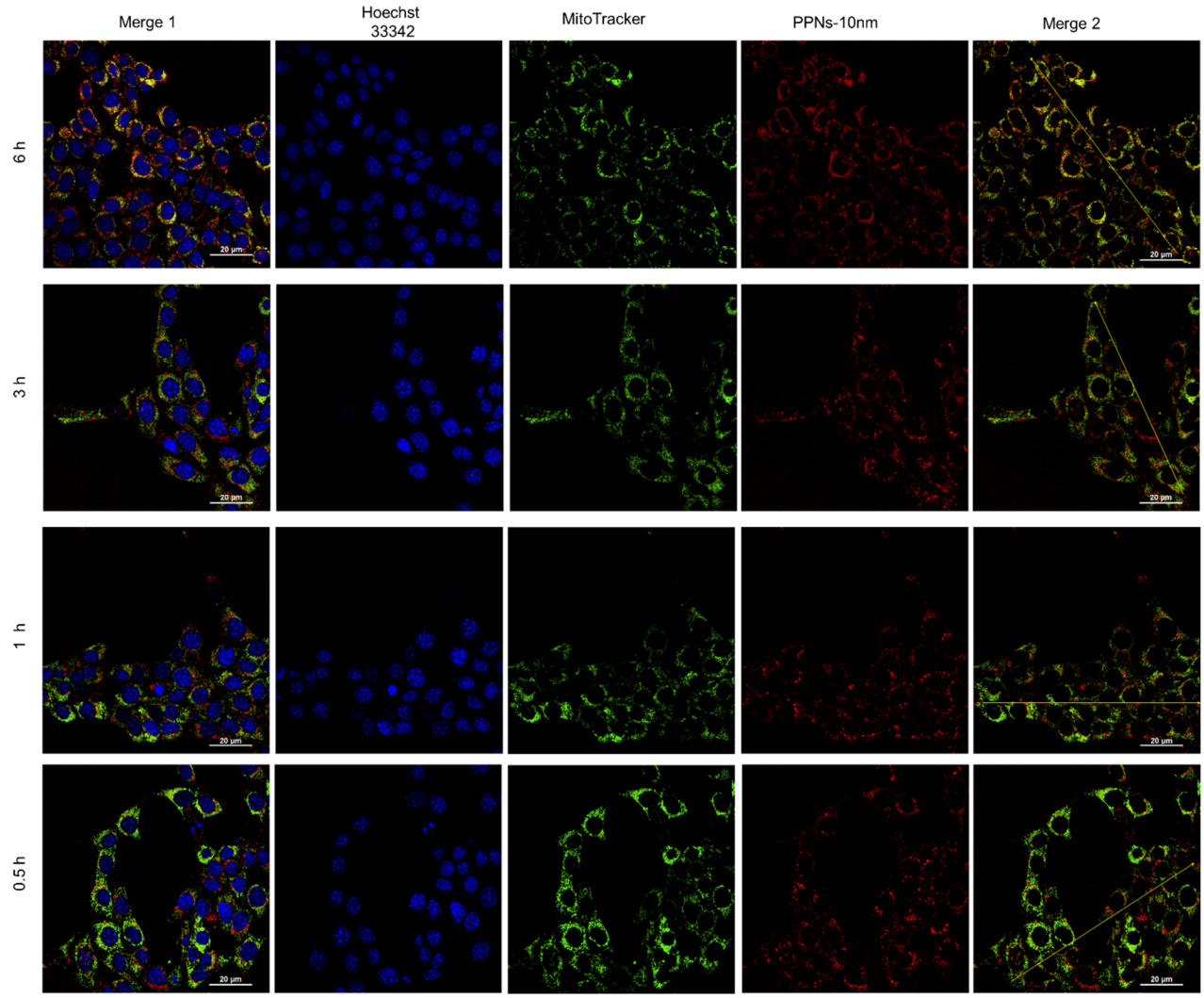

Figure S11. Confocal microscopy images of 4T1 cells treated with PPNs-10nm and treated with commercial organelle trackers. Overlay images and co-localization analysis of cells stained with mitochondrial markers indicated that PPNs-10nm localized in mitochondria. Merge 1: Hoechst33342, Mitotracker green, and PPNs-10nm. Merge 2: Mitotracker green and PPNs-10nm, the corresponding analysis was shown in **Figure 2**e.

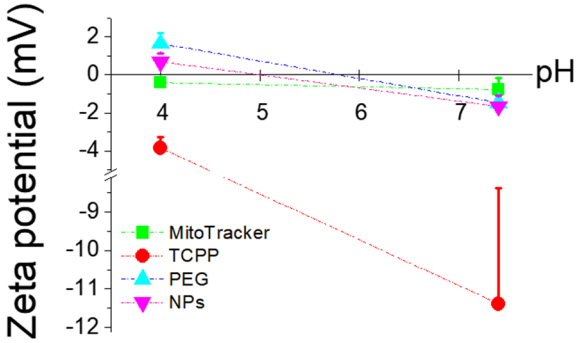

Figure S12. Zeta potential measurement. TCPP: mTCPP molecular dispersed in the buffer. PEG: aPEG dispersed in the buffer. NPs: PPNs-10nm. MitoTracker: MitoTracker green dispersed in buffer Lipophilic cations are one kind of mitochondrial probe and accumulate in the mitochondria, such as triphenylphosphonium, rhodamine 123 [3], and heptamethine cyanine dyes [4], because of its charge and solubility in the mitochondrial membrane and matrix space. Here, the mitochondrial localization of PPNs, which comprised of free amino and lipophilic cation rings are much more complex than the small molecule and might be due to the slightly positive surface potential.

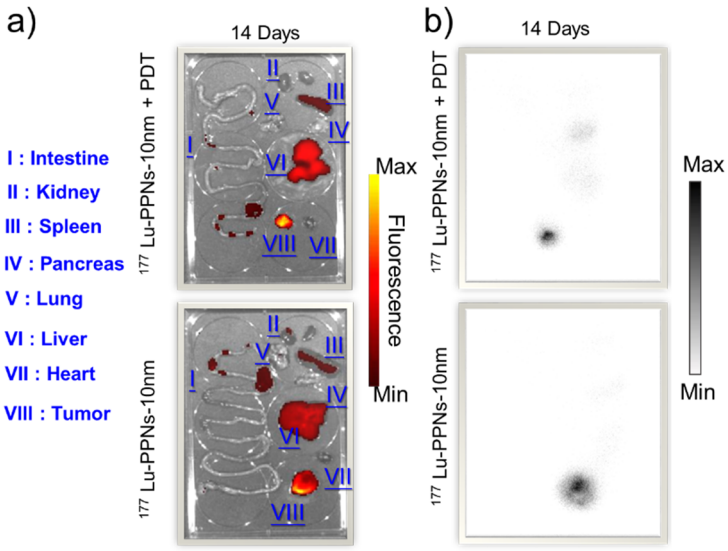

Figure S13. a) ex vivo fluorescence of harvested organs after 14 days p.i b) ex vivo gamma camera of harvested organs after 14 days p.i. Ex vivo imaging revealed that mTCPP fluorescence signals of both groups were primarily in the tumor.

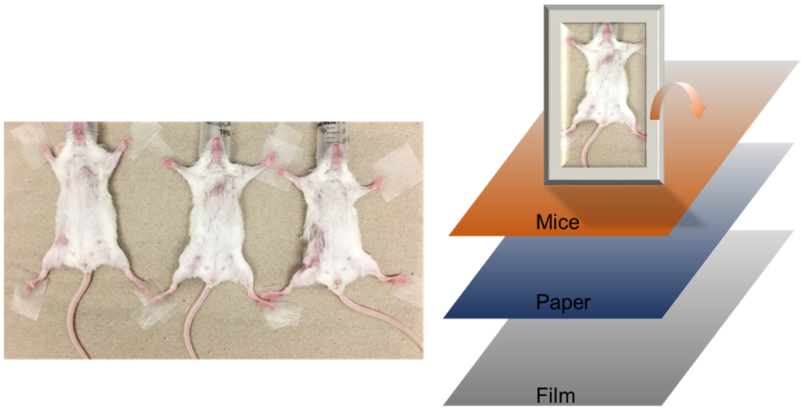

Figure S14. Schematic illustration of gamma camera imaging.

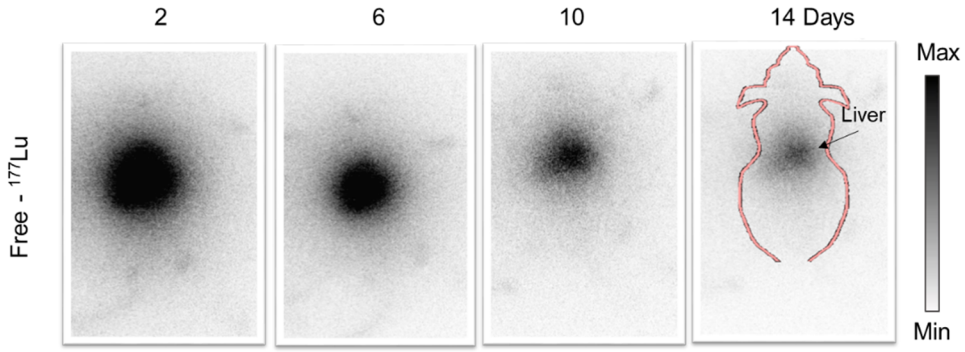

Figure S15. Gamma camera imaging of free ^{177}Lu after tail injection. The uptake of the two ^{177}Lu-PPNs-10nm groups in the liver was lower than that in the tumor. In contrast, the primary uptake of free ^{177}Lu were in the liver and spleen.

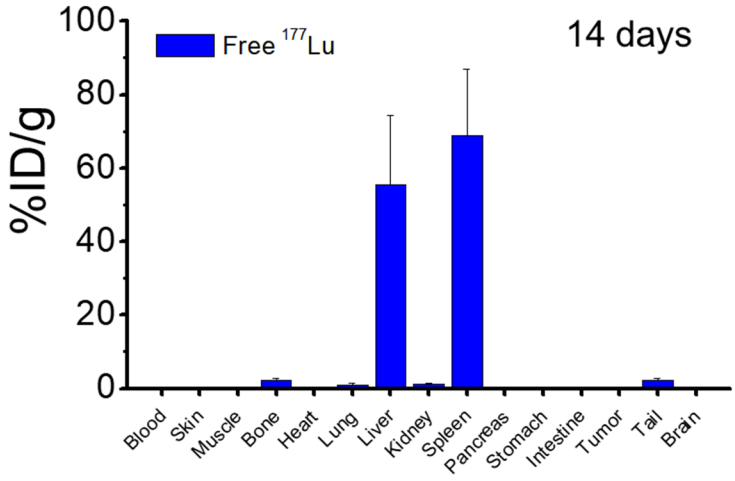

Figure S16. Biodistribution of free ^{177}Lu after 14 days p.i. The uptake of free ^{177}Lu in tumor, liver, and spleen was found to be 0.1 ± 0.03 %ID/g, 55.4 ± 19.0 %ID/g, and 68.9 ± 18.0 %ID/g, respectively (n=3).

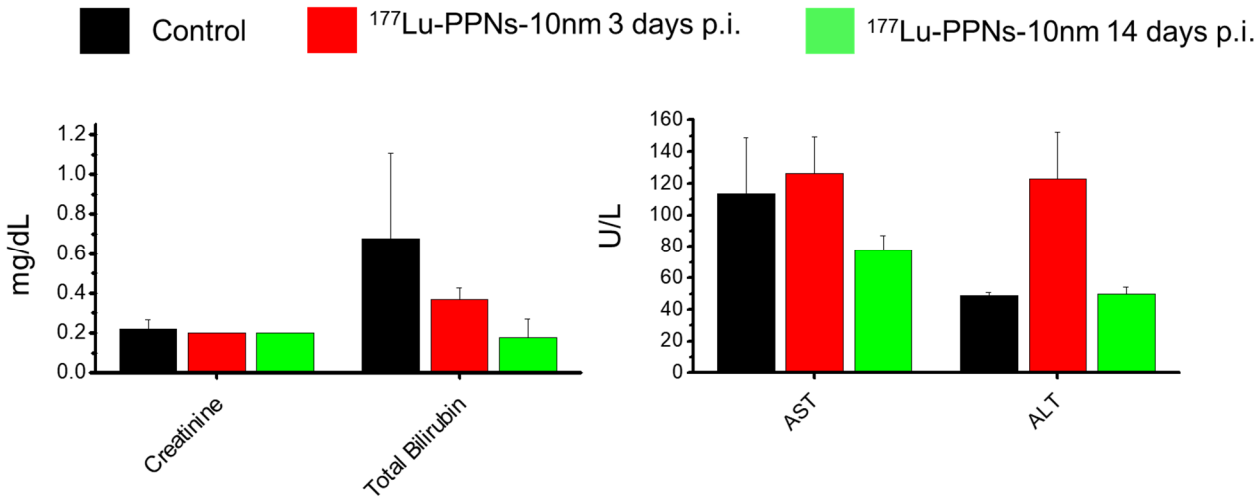

Figure S17. Serum biochemistry of liver and kidney. Healthy mice were intravenously injected with ^{177}Lu-PPNs-10nm or PBS. ALT presented aminotransferase and AST presented aspartate aminotransferase. It was found that ALT was higher than the control group at 3 days p.i. On day 14, no noticeable toxic side effects were found in the mice based on the serum biochemistry analysis. (n=3)

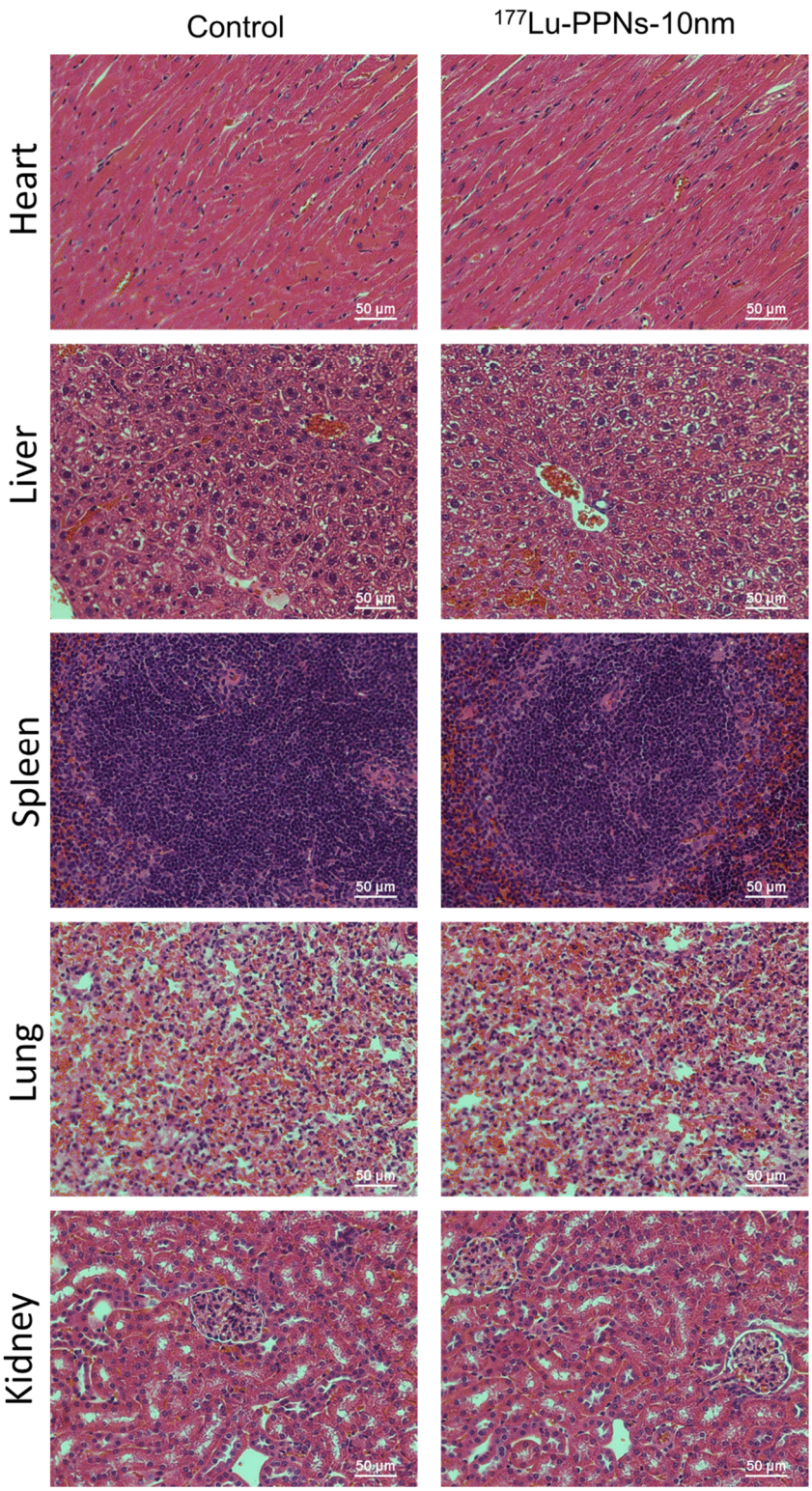

Figure S18. On Day 14, the major organs (i.e., heart, liver, spleen, lung, and kidneys) were sliced and stained with H&E for histology analysis. The results further demonstrate that there is no noticeable tissue damage in the main organs.

SUPPORTING INFORMATION

Author Contributions

Research design, data analysis, manuscript preparation: B.Y., Q.H. and W.C.

Experiments and data analysis: B.Y., H.W., C.A.F., C.J.K., D.N., Z.R., L.C., J.W.E.

Discussion and overseeing the collaborative project: F.Y., X.L., Q.H., W.C.

Q.H., X.L. and W.C. are the guarantors of this work and, as such, had full access to all the data in the study and take responsibility for the integrity of the data and the accuracy of the data analysis.

All authors approved the final manuscript.

Reference:

[1] H. Huang, R. Hernandez, J. Geng, H. Sun, W. Song, F. Chen, S. A. Graves, R. J. Nickles, C. Cheng, W. Cai, J. F. Lovell, *Biomaterials* **2016**, 76, 25-32.
[2] B. Yu, Y. Zhang, W. Zheng, C. Fan, T. Chen, *Inorg. Chem.* **2012**, 51, 8956-8963.
[3] R. C. Scaduto, Jr., L. W. Grotyohann, *Biophys. J.* **1999**, 76, 469-477.
[4] S. Luo, X. Tan, S. Fang, Y. Wang, T. Liu, X. Wang, Y. Yuan, H. Sun, Q. Qi, C. Shi, *Adv. Funct. Mater.* **2016**, 26, 2826-2835.